

Ultrashallow acceptors in neutron-transmutation-doped silicon

M. K. Udo, C. R. LaBrec,* and A. K. Ramdas

Department of Physics, Purdue University, West Lafayette, Indiana 47907

(Received 4 February 1991)

An additional series of excitation lines occurs in Si(B) subjected to slow-neutron irradiation and a partial high-temperature anneal. The neutron irradiation produces P by the transmutation of ^{30}Si and radiation damage due to the transmutation process itself as well as the unavoidable fast-neutron component of the neutron flux. The spacings and the relative intensities of the lines in the spectrum are strikingly similar to the excitation spectrum of boron acceptors in Si but with lower energies. This series corresponds to an acceptor (referred to as B_{NTD} , where NTD denotes neutron-transmutation doping) with a binding energy $E_I(B_{\text{NTD}})=28.24$ meV, significantly lower than $E_I(B)=45.70$ meV. The concentration of these ultrashallow acceptor centers increases with annealing in the temperature range 550–675 °C; at higher temperatures, these centers are annealed out. On the basis of piezospectroscopy, a tetrahedral (T_d) site symmetry is deduced for these centers and the deformation-potential constants of the ground state are determined. It appears that these acceptor centers are boron impurities in substitutional sites in association with defects. We have also discovered the analogous ultrashallow acceptors in which Al rather than B are involved.

I. INTRODUCTION

The physics of shallow donors and acceptors is a central theme in the field of semiconductors; through the effective-mass theory, it involves in an intimate manner the electronic band structure of the host—the nature of the conduction-band minima for donors and that of the valence-band maximum for acceptors.¹ Solid-state electronics and infrared sensors based on semiconductor technology depend rather crucially on the controlled introduction of known impurities. Thus the procedures for “doping” play an important role in the fabrication of a semiconductor of desired characteristics; equally, the theoretical understanding of the electronic energy levels of donors and acceptors, including the “chemical” nature of the ground state, is clearly essential. While electrical measurements provide the location of the ground states of the donors and acceptors in the forbidden gap, a complete energy-level scheme is established only from spectroscopic measurements. From a study of the Lyman spectra observed in the infrared, the $1s$ -like ground-state multiplet and a large number of p -like excited states have been discovered for group-V donors and group-III acceptors in Si and Ge. Comprehensive theoretical calculations have also provided binding energies and wave functions which are in excellent agreement with the experimental observations.¹

Despite the successes noted above, it should be emphasized that crystal-growth technology is not entirely under control as far as documenting and delineating all the impurities which might be present in a given crystal grown by a technique apparently under controlled conditions. Unexpected surprises occur—such as the introduction of oxygen in Si grown by the Czochralski technique involving quartz crucible and the subsequent generation of “thermal” donors as a result of unspecified annealing history.^{2,3} There is thus a strong, persistent interest in

exploring and implementing growth techniques and inventing procedures for the introduction of a desired “dopant.” Conventionally, impurities are introduced in the crystal during its growth process as dopants added to the melt in the Czochralski method or in the form of a suitable gaseous compound allowed to enter the vacuum chamber in which the crystal is grown by the floating-zone technique.⁴ Diffusion at high temperatures followed by a quench has been effective in introducing Li, Cu, and Mg into Si and Ge.⁵ Ion implantation followed by thermal or laser annealing is another strategy which has worked in a number of cases.⁶ Liquid-phase epitaxy, chemical-vapor deposition, and molecular-beam epitaxy—are examples of nonequilibrium growth techniques where there have been successes in incorporating impurities normally difficult to introduce. *In this context one of the most interesting techniques is based on nuclear reactions which transmute a host nucleus into a desired dopant nucleus.* The best example of this procedure is neutron-transmutation doping (NTD).

In the NTD technique as applied to Si, an undoped, high-purity crystal (presumably free from all defects) is exposed to slow neutrons from a nuclear reactor. As a result of the transmutation of ^{30}Si into ^{31}Si by neutron capture, and a subsequent β decay into ^{31}P , the crystal is doped with phosphorus donors. Based on the isotope abundance, the known cross section of the ^{30}Si isotope for neutron capture and the slow-neutron flux, the donors can be introduced in a known concentration. The unavoidable radiation damage, arising from the nuclear reactions and the fast-neutron component of the flux, is removed by resorting to an annealing at a sufficiently high temperature. Jagannath, Grabowski, and Ramdas⁷ have reported the observation of the Lyman spectrum of Si doped with P using NTD. Their work also focused on linewidths of the optical transitions, both natural as well as that resulting from the presence of charged defects.

We have investigated the corresponding aspect involving boron acceptors, namely, the introduction of phosphorus by NTD into an initially boron-doped Si sample, and with the concentration of boron larger than that of the phosphorus generated by NTD. After the appropriate annealing in order to remove the defects introduced by radiation damage, the typical boron spectrum corresponding to the excitation from the ground to the various excited states was observed.

We have performed a systematic investigation of the evolution of the excitation spectrum of boron in the presence of charged defects as a function of the annealing history of the Si sample. During the course of such studies we observed, in addition to the typical boron spectrum, *another set of acceptorlike excitation lines very similar to those of boron, but located at significantly lower energies.*⁸ In this paper we report the discovery of these acceptor centers, their growth and disappearance with annealing, and their symmetry as revealed in their piezospectroscopy.

II. EXPERIMENTAL PROCEDURE

The Lyman spectra of shallow centers in semiconductors typically lie in the far-infrared region between 20-100 μm (100–500 cm^{-1}), an ideal range for a Fourier-transform spectrometer. In the present investigation we employed a Beckman-RIIC FS-720 spectrometer⁹ in which the fixed mirror has been moved by 5 cm so as to obtain one-sided interferograms with a maximum path difference of 10 cm, thus allowing for a maximum unapodized resolution of 0.025 cm^{-1} . A liquid helium cooled Ge bolometer¹⁰ was used as a detector. The data acquisition and processing was performed with a Zenith Data Systems¹¹ Model Z-100 microcomputer running the MS-DOS operating system. In view of the small ionization energies of interest, the measurements were performed with samples cooled to liquid helium temperature to deionize the impurities. The details of the optical cryostat used in the present studies are given by Fisher *et al.*;¹² the sample is attached to a copper tailpiece which is in contact with liquid helium. Special precautions were taken to avoid straining the sample during mounting and cooling. In order to perform uniaxial stress measurements, the glass center piece is replaced by a stainless steel stress centerpiece, fully described by Tekippe *et al.*¹³ Due to reflections at the beamsplitter, together with its disposition in the spectrometer, the incident beam is partially polarized with its vertical component ~ 3.6 times stronger than the horizontal. For measurements in which the polarization of the incident beam is important, a polarization rotator¹⁴ is used. This device allows one to rotate the stronger vertical component of the incident beam to the desired direction of polarization. A Perkin-Elmer wire-grid polarizer¹⁵ was mounted on the cryostat window so that measurements could be made with the electric vector \mathbf{E} linearly polarized in the desired direction.

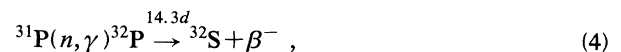
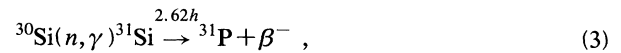
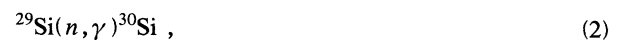
The samples used in the present study were cut from ingots conventionally doped with the group-III impurity during the floating-zone growth. The phosphorus donors

were introduced by the NTD technique¹⁶ and the annealing was performed in an atmosphere of flowing helium gas. For uniaxial stress measurements the samples were oriented along the [001] and [111] directions using the x-ray technique. Typical dimensions for the samples are $20 \times 8 \times 1 \text{ mm}^3$ for zero stress and $18 \times 5 \times 2 \text{ mm}^3$ for the uniaxial stress measurements, the long dimension being the direction of compression. A wedge of $\sim 50 \mu\text{m}$ was intentionally introduced along the length of the sample to eliminate interference effects, also known as "channeling." The optical surfaces were prepared by grinding with carborundum of successively finer grit, followed by polishing with 3 μm diamond paste and 0.05 μm alumina. Finally, a chemical etch was used to remove the surface damage caused by the mechanical polishing. During sample preparation special care was taken to maintain the desired crystallographic directions.

III. NEUTRON TRANSMUTATION DOPING (NTD)

As remarked in the Introduction, nuclear transmutation is a procedure which can be exploited successfully in specific semiconductors. Lark-Horovitz¹⁷ recognized the feasibility of transmutation doping of semiconductors and demonstrated it with studies on Ge. He also drew attention to the nuclear reactions $^{30}\text{Si}(n, \gamma)^{31}\text{Si} \rightarrow ^{31}\text{P}$ and $^{28}\text{Si}(n, 2n)^{27}\text{Si} \rightarrow ^{27}\text{Al}$, the former with slow neutrons and the latter with fast neutrons. In recent years NTD of Si and GaAs with slow neutrons has been successfully exploited. The occurrence of appropriate isotopes which can transmute to a desired dopant, the cross section for such transmutation, and the slow-neutron flux of the current reactors represent the constraints on this technique.

The first systematic NTD studies of Si were performed by Tanenbaum and Mills.¹⁸ NTD in Si is based on the nuclear transmutation of ^{30}Si into ^{31}P . In Table I we list the natural abundance of the various isotopes of Si. The nuclear reactions involving thermal-neutron capture in Si are



where n , γ , and β^- denote a thermal neutron, a γ ray, and a β particle, respectively; the half lives of the unstable products are listed above the arrows, with the decay

TABLE I. Natural abundances (in %) and cross sections (in barns) for thermal neutron capture for the isotopes of Si and P.

| Natural abundance (%) | Isotope | Cross section $\sigma(n, \gamma)$ |
|-----------------------|------------------|-----------------------------------|
| 92.27 | ^{28}Si | $0.08 \pm 0.03 \text{ b}$ |
| 4.68 | ^{29}Si | $0.28 \pm 0.09 \text{ b}$ |
| 3.05 | ^{30}Si | $0.11 \pm 0.01 \text{ b}$ |
| 100 | ^{31}P | $0.20 \pm 0.02 \text{ b}$ |

products to the right. Equation (3) describes the specific reaction that generates ^{31}P , the desired dopant. The production of ^{32}S is an undesired side effect, but since it is formed as a second-order by-product, the final concentration is negligibly small. However, it is this reaction, with a half-life of 14.3 days, that causes most of the lingering radioactivity after irradiation, requiring a "cool-down" period before the crystal can be safely handled. The rate of production R of a given isotope is a function of the amount initially present N_T (typically corresponding to its natural abundance), the cross section for thermal-neutron capture σ , and the thermal-neutron fluence Φ :

$$R = N_T \sigma \Phi . \quad (5)$$

The thermal-neutron-capture cross sections for the Si isotopes are also listed in Table I.

It is useful to note here some of the limitations of the NTD technique. For Si, the desired dopant ^{31}P is the result of the transmutation of the least abundant isotope ^{30}Si (abundance 3.05%). With a nominal thermal-neutron flux of $\sim 10^{13}$ neutrons per cm^2 per second, and the known cross section for $^{30}\text{Si}(n, \gamma)^{31}\text{Si}$, ^{31}P is created at the rate of $\sim 6 \times 10^{12}$ per hour. In order to achieve concentrations of $\sim 10^{16} \text{ cm}^{-3}$ or higher, inordinately large irradiation times will thus be necessary, e.g., a concentration of $\sim 10^{16} \text{ cm}^{-3}$ requires about 69 days, while 10^{18} cm^{-3} would take ~ 19 years.

There are two main advantages of NTD over conventional doping techniques. One is the accuracy with which the dopant concentration can be known. The final ^{31}P concentration is only a function of the thermal-neutron flux and the exposure time of the crystal to such flux. The accuracy of fluence measurement has been demonstrated to be better than $\pm 1\%$ by using, for example, a rhodium wire self-powered detector.¹⁹ The exposure time can be likewise controlled. The other advantage is that better homogeneity of the phosphorus donors is achieved, since the neutron-flux density can be made quite uniform. Thus, after complete annealing, a sample of highly uniform resistivity can be achieved.²⁰ In contrast to Ge, where some isotopes transmute to a donor and some to an acceptor, NTD Si is free from compensation.¹⁷

The NTD process, however, creates undesired side effects due to the "radiation damage" caused in the crystal. This damage stems from two major sources.²¹ When the target atoms undergo the γ and β decays, the recoil produced displaces the transmuted atom from its lattice site, and thus creates a defect near it. Also, the thermal-neutron flux is accompanied by an unavoidable flux of fast neutrons which cannot be completely eliminated; these fast neutrons collide with the atoms in the crystal, also displacing them from their original sites. The resulting defects are, in general, quite complicated, consisting of vacancy complexes, divacancies, vacancy clusters, and interstitials presumably in complexes as well as larger clusters and dislocation loops.²² The concentration of such defects depends on the ratio of fast to thermal-neutron flux to which the sample is exposed, on the energy spectrum of the fast neutrons, and on the temperature of the crystal during irradiation. The defects produced in

this manner are effective in trapping carriers and the acceptors already present or the P donors generated by NTD are completely compensated. By annealing^{22,23} the crystal at sufficiently high temperature for a sufficient length of time, these defects are removed and the attendant compensation eliminated.

IV. NTD IN Si(B)

Figure 1 shows the excitation lines of boron acceptors as a function of annealing for a sample containing an initial boron concentration of $\sim 1.5 \times 10^{15}$ and $\sim 1.0 \times 10^{14} \text{ cm}^{-3}$ phosphorus donors introduced by NTD; we denote samples prepared in this fashion as Si(B, P_{NTD}). After exposure to the slow neutrons and *before* annealing, defects generated by radiation damage create traps that completely compensate the acceptors, and as shown in Fig. 1, curve (a), no excitation lines are observed. As the annealing proceeds, radiation damage is removed along with the compensation it produces, and the $p_{3/2}$ spectrum associated with the neutral boron acceptors progressively manifests itself as can be seen in (b)–(d) of Fig. 1 at the various annealing stages indicated. Finally, after all the radiation damage is eliminated by the annealing, the $p_{3/2}$ series appears in full strength consistent with the compensation produced by the NTD generated substitutional phosphorus [see Fig. 1, curve (e)].

As has been remarked above, the NTD process introduces radiation damage; to the extent the defects are charged, one might expect electric-field-induced modifications of the widths and shapes of the excitation lines. In addition, one could also expect the local strains produced by defects to affect the energy positions and line shapes of the excitation lines of carriers bound to acceptors and/or donors. Jagannath, Grabowski, and Ramdas⁷ have studied the effect of charged defects on the line shapes and widths of the excitation spectrum of phosphorus donors introduced in silicon by NTD. They found a strong broadening and low-energy asymmetry of the excitation lines and attributed them to the quadratic Stark broadening, such effects being stronger for the states having larger orbits.

Figure 2, curve (a), shows the excitation spectrum of boron acceptors in silicon before the sample was subjected to slow-neutron irradiation. In addition to the boron lines we also see the $2p_0$ and $2p_{\pm}$ lines of residual phosphorus donors. This occurs because in our spectrometer unfiltered radiation including that with energy larger than the band gap of silicon is incident on the sample and some of the residual phosphorus get deionized by capturing electrons created by interband transitions. When a black polyethylene filter was placed before the sample to block the shorter wavelengths, the phosphorus lines disappeared. After exposing the boron-doped silicon to a flux of slow neutrons and annealing it for 10 h at 725 °C, we observed a strong broadening of the boron acceptor lines corresponding to the higher orbits, but no dramatic asymmetry was visible; such effects are illustrated in Fig. 2, curve (b). The $2p_0$ and $2p_{\pm}$ lines of phosphorus associated with the band-gap radiation referred to above are not observed in this case; the reason for this is not clear.

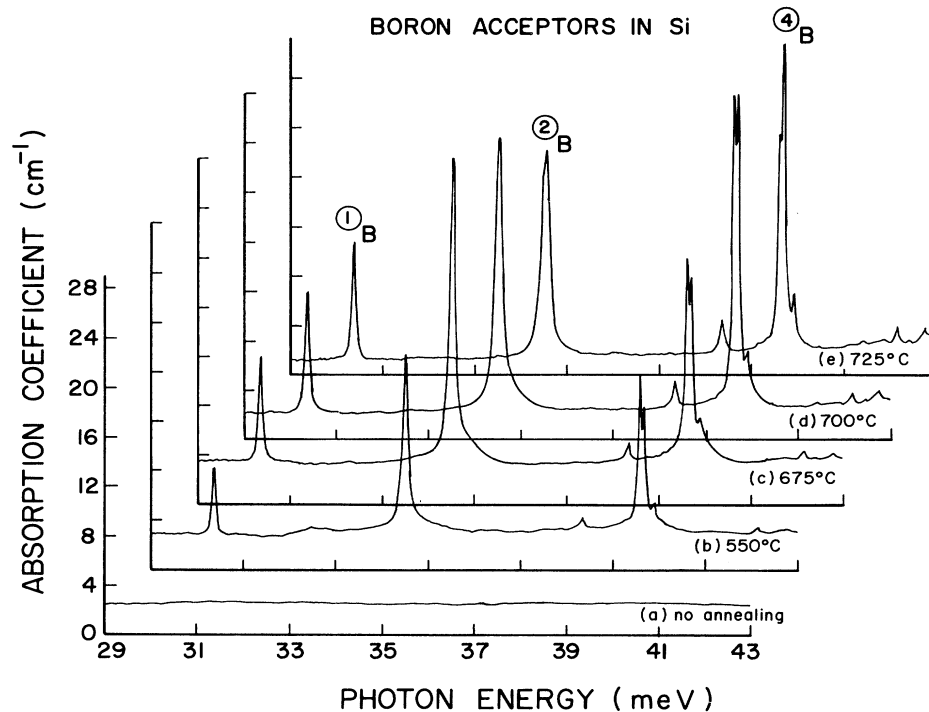


FIG. 1. Electronic excitation spectra of boron acceptors compensated by NTD generated phosphorus in $\text{Si}(\text{B},\text{P}_{\text{NTD}})$: (a) before any annealing; (b) after annealing for 27 h at 550°C; (c) after annealing for 16 h at 675°C; (d) after annealing for 20 h at 700°C and (e) after annealing for 10 h at 725°C. The spectra were recorded with liquid helium as the coolant.

During the course of this investigation, we discovered an *additional* series of excitation lines located at significantly *lower* energy than that of the $p_{3/2}$ series of boron acceptors. These excitation lines were initially observed after the first annealing at 500°C. In Fig. 3 we illustrate its evolution as a function of annealing. It is interesting to note that as the annealing temperature was increased, the intensity of these lines increased, reached a maximum, and then decreased. Finally, after annealing

for 10 h at 725°C, these lines disappeared completely as can be seen in Fig. 3, curve (e). In view of the striking resemblance between these lines and those corresponding to boron acceptors, we ruled out the possibility that they may be instrumental artifacts due to aliasing in the interferometer; the only source of aliasing would be due to features $\sim 1100\text{ cm}^{-1}$, a spectral region eliminated by the optical filters and windows used in our spectrometer. The complete disappearance of the series after all the annealing (in contrast to the boron spectrum which remains at full strength) is yet another evidence which rules out aliasing.

As is evident from a comparison of the excitation spectra of the boron acceptors and the NTD centers, they bear a striking resemblance. The intensities of the corresponding lines and their spacings are closely matched, indicating that the NTD centers are effective-mass acceptors and that their *excited* states *have the same* binding energies. The large separation of the spectral range where they occur signifies that their ground states have an appreciable *difference* in their binding energies. In fact, the ground state of the NTD centers has suffered a significantly large negative chemical shift with respect to the ground state of the group-III acceptors in silicon. The binding energies of the excited and ground states can be deduced following the same procedure as that employed for the group-III acceptors in silicon, in which the assumption is made that the effective-mass theory²⁴ gives accurately the binding energy of the final state of the line 4 transition as 6.1 meV. The binding energies deduced

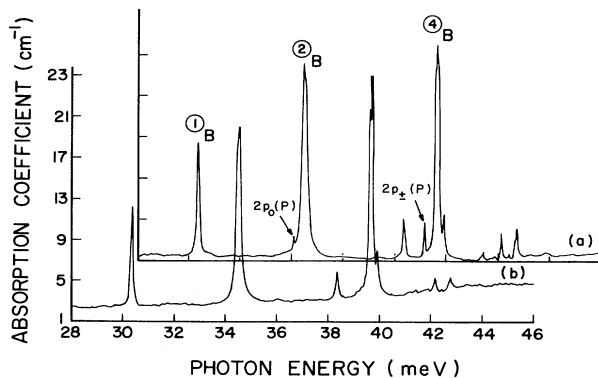


FIG. 2. Electronic excitation spectra of (a) boron acceptors in Si before neutron irradiation; (b) boron acceptors compensated by NTD phosphorus after annealing for 10 h at 725°C. Measurements were performed using liquid helium as coolant.

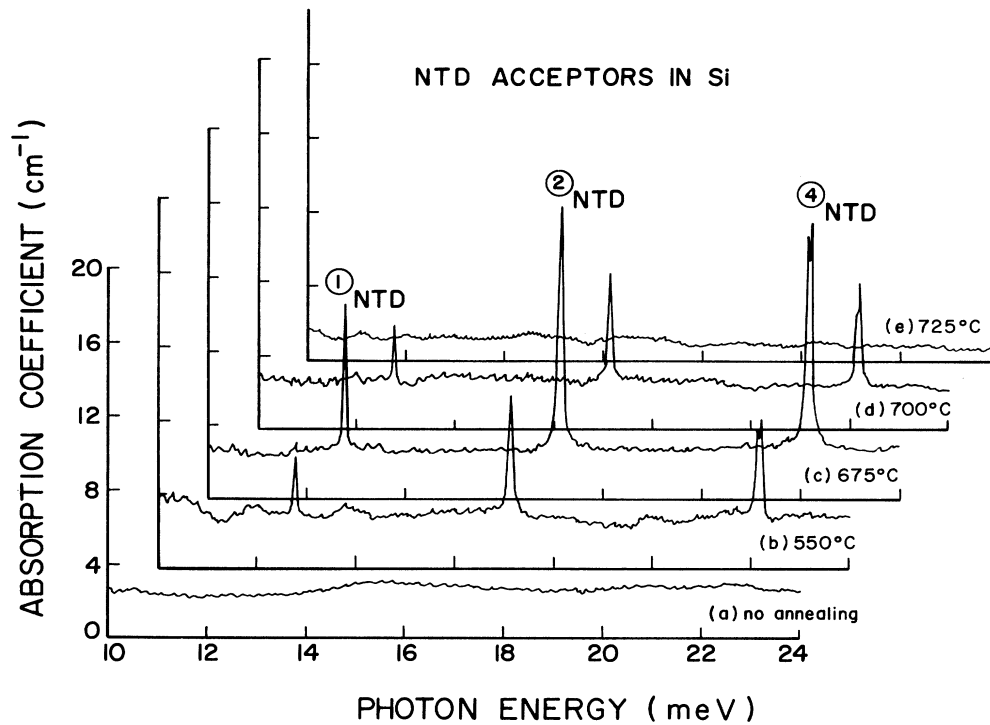


FIG. 3. Electronic excitation spectra of NTD acceptors in $\text{Si}(\text{B}, \text{P}_{\text{NTD}})$ (a) before any annealing, (b) after annealing for 27 h at 550°C, (c) after annealing for 16 h at 675°C, (d) after annealing for 20 h at 700°C, and (e) after annealing for 10 h at 725°C. Measurements were performed using liquid helium as coolant.

from the positions of the NTD lines are listed in Table II under the column B_{NTD} . The correspondence between these energies and those of the known acceptors suggests that they can be attributed to an acceptor center and will hereafter be denoted as B_{NTD} since it appears to be associated with boron, as we will see presently. We emphasize the extremely low ionization energy of B_{NTD} ground state $E_I(B_{\text{NTD}}) = 28.24$ meV as compared with that for B with $E_I(\text{B}) = 45.70$ meV. In order to discover if there are NTD centers associated with other group-III acceptors in silicon, we examined a sample of silicon containing $\sim 2.7 \times 10^{15} \text{ cm}^{-3}$ aluminum acceptors and

TABLE II. Experimentally deduced binding energies (in meV) of the final states of acceptors in silicon. The subscript NTD refers to the levels found in samples with the specified impurity. The values are calculated assuming the theoretical value of 6.1 meV predicted for line 4, with the exception of the ionization energy for Al, which is taken from Ref. 1. Maximum error estimated to be ± 0.01 meV.

| Line | B | B_{NTD} | Al | Al_X | Al_{NTD} |
|-------|-------|------------------|-------|---------------|--------------------------|
| 1 | 15.33 | 15.47 | 15.27 | 15.41 | 15.70 |
| 2 | 11.19 | 11.10 | | 11.21 | 11.14 |
| 3 | 7.34 | | | | |
| 4 | 6.1 | 6.1 | | 6.1 | 6.1 |
| 4A | 5.79 | | | | |
| 4B | 6.03 | 6.04 | | 6.04 | |
| E_I | 45.70 | 28.24 | 70.18 | 57.33 | 43.25 |

$\sim 1.0 \times 10^{14} \text{ cm}^{-3}$ NTD-induced phosphorus donors. Figure 4 shows the portion of spectrum containing excitation lines due to Al and the so-called "X centers", Al_X ; only line 1 of the Al acceptor is observed in the spectral range accessible with the combination of windows, filters, and beamsplitter employed. The binding energies of the levels involved are shown in Table II under Al and Al_X . The lower energy portion of this spectrum, shown in Fig. 5, contains lines which can be associated with Al_{NTD}

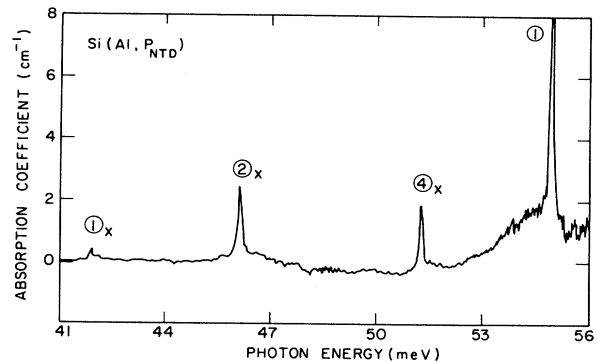


FIG. 4. Electronic excitation spectrum of Al acceptors compensated by NTD phosphorus in $\text{Si}(\text{Al}, \text{P}_{\text{NTD}})$ after annealing for 10 h at 600°C; Al_X centers are identified with the subscript X. Measurements were performed using liquid helium as coolant.

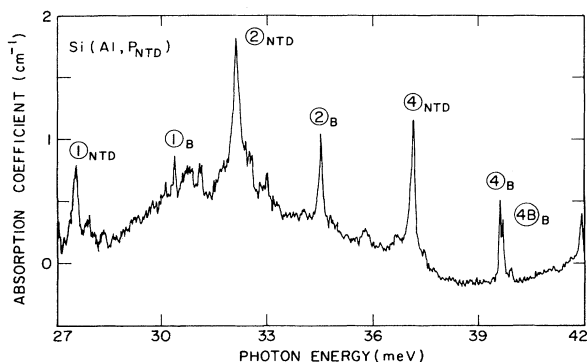


FIG. 5. Electronic excitation spectrum of Al_{NTD} acceptors compensated by NTD generated phosphorus in $\text{Si}(\text{Al}, \text{P}_{\text{NTD}})$ after annealing for 10 h at 600°C . Lines labeled with subscript B are due to the residual boron centers, while those of $\text{Si}(\text{Al}, \text{P}_{\text{NTD}})$ are identified with subscript NTD. Measurements were performed using liquid helium as coolant.

centers. The binding energies of their final states are listed in Table II under the column Al_{NTD} . Also present in the spectrum are transitions due to boron acceptors in the sample, known to occur as “residual” impurities in most silicon.²⁵ We note that the B_{NTD} lines occur in $\text{Si}(\text{B})$ subjected to neutron-transmutation doping, i.e., in $\text{Si}(\text{B}, \text{P}_{\text{NTD}})$ but not in $\text{Si}(\text{Al}, \text{P}_{\text{NTD}})$, whereas the corresponding Al_{NTD} lines appear in $\text{Si}(\text{Al}, \text{P}_{\text{NTD}})$ but not in $\text{Si}(\text{B}, \text{P}_{\text{NTD}})$. Furthermore, there is a very good correspondence in the ratio between the ionization energies of the NTD and the parent group-III acceptor for both impurities, viz. $E_I(\text{B}_{\text{NTD}})/E_I(\text{B})=0.618$ and $E_I(\text{Al}_{\text{NTD}})/E_I(\text{Al})=0.616$. These ratios appear to indicate that the NTD center is related to the specific group-III acceptor present in silicon. Evidence for shallow acceptor centers in NTD silicon originally doped with Al, In, and Ga has also been found by Young, Marsh, and Baron²⁶ in their Hall effect measurements. They reported two shallow levels denoted E_1 and E_2 , with ionization energies 30 and 41 meV, 31 and 45 meV, and 27 and 39 meV, for $\text{Si}(\text{Al})$, $\text{Si}(\text{In})$, and $\text{Si}(\text{Ga})$, respectively. It is interesting to note that for the three impurities that they measured, a level was found around 27–31 meV; it could be associated with B_{NTD} resulting from the residual boron²⁵ in their Si as suggested by our systematic annealing study on $\text{Si}(\text{B}, \text{P}_{\text{NTD}})$ and $\text{Si}(\text{Al}, \text{P}_{\text{NTD}})$. The values reported for the E_2 level, 39–45 meV, are consistent with the more precise determination of the ionization energy of the Al_{NTD} center, viz., 43.25 meV found in the present work. Young, Marsh, and Baron²⁶ also reported the disappearance of the shallow centers for the gallium-doped sample at an annealing temperature $\sim 700^\circ\text{C}$. This result is in agreement with our findings on $\text{Si}(\text{B}, \text{P}_{\text{NTD}})$, where only the boron acceptor excitations were observed in a sample that was completely annealed. Furthermore, we established that NTD levels are not observed in as-grown $\text{Si}(\text{B})$, even when annealed. It appears that the NTD acceptor center is a complex formed between the group-III impurity and a radiation-induced defect.

At this point it is useful to review the characteristics of a defect center, known as the X center, discovered in the course of optical investigations of group-III acceptors in silicon. An observation of such X centers has been made by Onton, Fisher, and Ramdas²⁷ on crucible grown $\text{Si}(\text{Al})$ where, in addition to the Al excitation lines, they saw an additional set of lines Al_X located at energies lower than those of Al. A more detailed investigation on the Al_X center was performed by Chandrasekhar and Ramdas,²⁸ using piezospectroscopy they established that the X center has a trigonal rather than a tetrahedral symmetry, the preferred axis being along $\langle 111 \rangle$. However, the nature of the complex insofar as which impurity is involved has yet to be conclusively determined. Analogous X centers have also been observed in $\text{Si}(\text{B})$, $\text{Si}(\text{In})$, and $\text{Si}(\text{Ga})$ by Jones *et al.*;²⁹ they reported a “defect spectrum” associated with each of the impurities, at energies smaller than that of the substitutional group-III impurity. The ratio of the ionization energy of the X center and the associated group-III impurity has been found to be 0.84 for B, 0.82 for Al, 0.79 for Ga, and 0.72 for In, indicating that for each group-III acceptor there is a corresponding X center. We emphasize that NTD centers are *not* X centers; the boron-related X -center B_X has an ionization energy $E_I(\text{B}_X)=38.46$ meV, a value quite distinct from that for B_{NTD} with $E_I(\text{B}_{\text{NTD}})=28.24$ meV. We also note that, after annealing at sufficiently high temperature, the lines corresponding to the X centers have been reported to be still strongly visible,²⁹ while those corresponding to the NTD centers disappear as shown in the present study. From all the above findings, it appears that a convincing case can be made that the ultrashallow NTD acceptor centers are a different kind of acceptor complex involving a group-III impurity in silicon and a radiation-induced defect.

V. SYMMETRY OF NTD CENTERS: PIEZOSPECTROSCOPY

In the preceding section we described the discovery of the ultrashallow NTD acceptor centers and the remarkable similarity between their excitation lines and those corresponding to boron acceptors. On the basis of the spacing between the lines and their intensities, it is clear that the excited states are well described by the effective-mass theory as successfully applied to group-III acceptors in silicon.¹ It is of interest to determine the site symmetry of this acceptor center and compare it with that of the other defects or impurities present in silicon. For example, all the group-III acceptors in silicon possess tetrahedral (T_d) site symmetry while the X centers of aluminum have trigonal site symmetry with the preferred axes along $\langle 111 \rangle$ and the associated orientational degeneracy.^{28,29}

A. Theoretical considerations

Under an external stress the site symmetry of an impurity in a crystal is lowered, in general, resulting in the removal of degeneracy of its energy levels. From the stress-induced splittings, shifts, and polarization charac-

teristics of the components of the spectral lines of the impurity, i.e., on the basis of its piezospectroscopy, one can establish level degeneracies and deduce the irreducible representation(s) to which a given energy state belongs. Indeed, piezospectroscopy has been successfully exploited in the context of the electronic states of donors and acceptors in silicon and germanium and has proved to be a valuable tool in identifying their *site symmetry*,¹ by performing quantitative stress measurements the *deformation-potential constants* characterizing both the ground and excited states can be deduced.

In order to interpret piezospectroscopic effects, we recall¹ that the acceptor states reflect the degeneracy of the $\Gamma_8^+(p_{3/2})$ and the $\Gamma_7^+(p_{1/2})$ valence-band maxima. For compressive force, \mathbf{F} , in an arbitrary direction, the Γ_8^+ quadruplet state shifts and splits into two Kramers doublets whereas the Γ_7^+ , a Kramers doublet, merely shifts. A substitutional group-III acceptor in silicon, such as boron, has energy levels which can be classified according to the double-valued irreducible representation³⁰ of its site symmetry group T_d , viz., Γ_6 , Γ_7 , or Γ_8 . Of these, Γ_6 and Γ_7 are doublets, whereas Γ_8 is a quadruplet. In the effective-mass approximation the ground state of the acceptor is a $\Gamma_8(\bar{T}_d)$ level. For $\mathbf{F} \parallel [111]$ the T_d site symmetry reduces to C_{3v} , whereas for $\mathbf{F} \parallel [001]$ it reduces to D_{2d} . Both $\Gamma_6(\bar{T}_d)$ and the $\Gamma_7(\bar{T}_d)$ states transform to $\Gamma_4(\bar{C}_{3v})$ for $\mathbf{F} \parallel [111]$, whereas for $\mathbf{F} \parallel [001]$, they are $\Gamma_6(\bar{D}_{2d})$ and $\Gamma_7(\bar{D}_{2d})$, respectively. The states belonging to Γ_6 and Γ_7 of \bar{T}_d do not split further under stress, but shift from their zero-stress position, the shift being isotropic with respect to the direction of \mathbf{F} . For Γ_6 states, this shift is given by $\Delta E(\Gamma_6) = A(s_{11} + 2s_{12})T$, where A is the deformation-potential constant, s_{ij} 's are the elastic compliance constants, and T is the applied force \mathbf{F} per unit area, defined to be *negative for compression*. A similar result holds for a Γ_7 level. For $\mathbf{F} \parallel [111]$ the stress-induced sublevels originating from a Γ_8 state, either the ground or an excited, are $\Gamma_5 + \Gamma_6$ and Γ_4 where the irreducible representations belong to \bar{C}_{3v} . For $\mathbf{F} \parallel [001]$, $\Gamma_8(\bar{T}_d)$ decomposes into Γ_6 and Γ_7 of \bar{D}_{2d} . The eigenvalues corresponding to these stress-induced sublevels are given in Table III. The Γ_8 states split by $(d/\sqrt{3})s_{44}T$ and by

TABLE III. Symmetries and eigenvalues of the stress-induced sublevels of a Γ_8 state for $\mathbf{F} \parallel [111]$ and $\mathbf{F} \parallel [001]$, where \mathbf{F} is the applied force.

| Direction of \mathbf{F} | State | Eigenvalue |
|---------------------------|---|---|
| | $\Gamma_5(\bar{C}_{3v}) + \Gamma_6(\bar{C}_{3v})$ | $a(s_{11} + 2s_{12})T + (d/2\sqrt{3})s_{44}T$ |
| [111] | $\Gamma_4(\bar{C}_{3v})$ | $a(s_{11} + 2s_{12})T - (d/2\sqrt{3})s_{44}T$ |
| | $\Gamma_6(\bar{D}_{2d})$ | $a(s_{11} + 2s_{12})T + b(s_{11} - s_{12})T$ |
| [001] | $\Gamma_7(\bar{D}_{2d})$ | $a(s_{11} + 2s_{12})T - b(s_{11} - s_{12})T$ |

$2b(s_{11} - s_{12})T$ for $\mathbf{F} \parallel [111]$ and $\mathbf{F} \parallel [001]$, respectively, where d and b are the corresponding shear deformation-potential constants; the subscripts of b and d identify the specific Γ_8 state, e.g., b_0 and d_0 characterize the $\Gamma_8(p_{3/2})$ ground state.

The stress-induced splitting of the $\Gamma_8 \rightarrow \Gamma_8$, $\Gamma_8 \rightarrow \Gamma_6$, and $\Gamma_8 \rightarrow \Gamma_7$ transitions for $\mathbf{F} \parallel [111]$ and $\mathbf{F} \parallel [001]$ are shown in Fig. 6. The figure also shows the selection rules for electric-dipole transitions, with the dashed arrows corresponding to transitions with the electric vector, \mathbf{E} , parallel to \mathbf{F} while the full arrows are for $\mathbf{E} \perp \mathbf{F}$. From such a diagram we can predict the splittings, the level-crossing effects when sublevels of the same symmetry cross each other under stress and dichroism of the stress-induced components of a given electric-dipole transition. In addition, the ground-state splitting results in the depopulation of the upper ground state with increasing stress and decreasing temperatures. By appealing to the experimental observations based on the polarization features

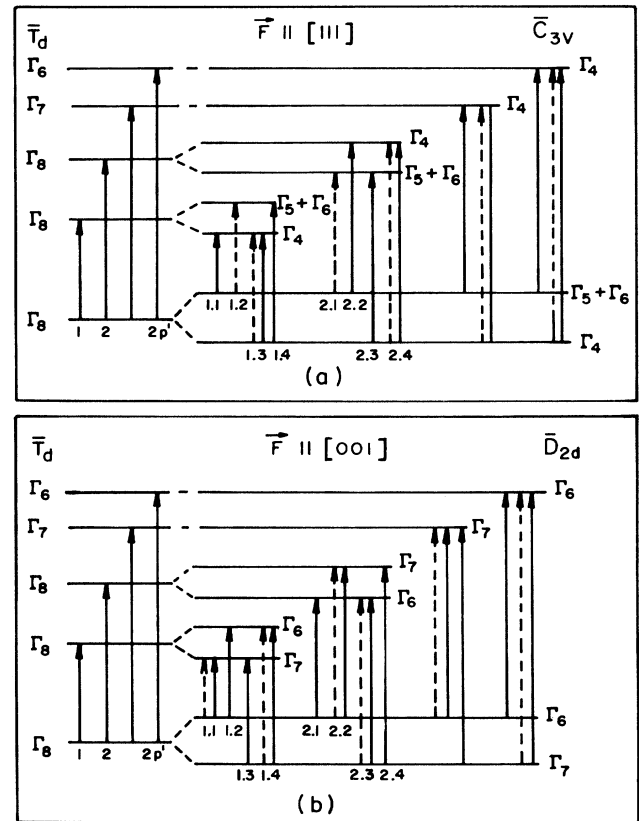


FIG. 6. The allowed transitions from a Γ_8 ground state to Γ_6 , Γ_7 and Γ_8 excited states of the double group \bar{T}_d with compressive force \mathbf{F} along (a) [111] for which the site symmetry under stress is C_{3v} or (b) [001], where the site symmetry is D_{2d} . The designations next to the levels denote the irreducible representations of the appropriate double point group following the notation of Koster *et al.* (Ref. 30). The dashed arrows are for the electric vector $\mathbf{E} \parallel \mathbf{F}$ while the full arrows are for $\mathbf{E} \perp \mathbf{F}$.

and the depopulation effects, the energy ordering of the sublevels are deduced or, equivalently, the sign of the deformation-potential constant characteristic of the splitting. The quantitative stress dependence of the energies of the stress-induced components yields the relevant deformation-potential constants.

We note that crystal-field effects may manifest themselves in the observed optical transitions if the site symmetry of the impurity is lower than T_d . In that case, the Γ_8 ground state will split into two Kramers doublets even in the absence of an external stress. If this crystal-field-induced splitting of the ground state is too small to be resolved experimentally, then, one may not be able to distinguish the lower symmetry of the impurity from the tetrahedral symmetry. On the other hand, if the magnitude of the crystal-field splitting is such that the upper Kramers doublet cannot be thermally populated, then no additional structure will arise in the optical transitions originating from the presence of two ground states at zero stress. For a small but finite splitting of the ground state, we expect to see the optical transitions corresponding to both the upper and lower Kramers doublet but the uniaxial stress will not split them further, and only depopulation effects will be observed as they move apart. Experimental observations on the NTD acceptors do not reveal any additional structure at zero stress. We therefore assume that the NTD acceptor has either a T_d symmetry or a crystal-field-split pair of ground states, one of which lies at an energy $\gg kT$ above the other.

If the NTD center has effective-mass-like excited states but a Kramers doublet as a ground-state characteristic of a site symmetry lower than T_d , then one has to take into account the effects of orientation degeneracy when uniaxial stress is applied. As an illustrative example, consider a defect with its symmetry axis along $\langle 100 \rangle$. Assuming a random distribution of these defects in the crystal, one expects equal numbers of centers with their symmetry axes pointing along $[100]$, $[010]$, and $[001]$ as a result of this "orientational degeneracy" and, at zero stress, they collectively exhibit isotropic optical transitions. For $F\parallel[001]$, the ground state of the defects along $[001]$ suffers a shift different from those of the defects along $[010]$ and $[100]$. For $F\parallel[110]$ the defects oriented along $[100]$ and $[010]$ should exhibit identical shifts of their ground states whereas the ground state of the species along $[001]$ should shift differently; however, for $F\parallel[111]$ the ground states of the species along $[100]$, $[010]$, and $[001]$ are all expected to shift identically. If the symmetry axis of the defects were to be along $\langle 110 \rangle$, $F\parallel[001]$, $[110]$, and $[111]$ would result in two, three, and two $\langle 110 \rangle$ subgroups, respectively, classified according to their ground-state shifts. For orientational degeneracy along $\langle 111 \rangle$ there would be no regrouping for $F\parallel[001]$ and two subgroups for $F\parallel[110]$ or $[111]$. These results are summarized in Table IV. If the acceptor center has even lower symmetry, one can show that effects associated with the removal of orientational degeneracy and, in turn, a rather large number of subgroups will be seen for any direction of F . Thus, results for $F\parallel[001]$ and $F\parallel[111]$ are sufficient to expose the latent anisotropy concealed by the orientational degeneracy; one should

TABLE IV. Removal of the orientational degeneracy of non-cubic centers under uniaxial compression.

| Direction of compressive force, F | Number of subgroups under compression | | |
|-------------------------------------|---------------------------------------|-----------------------|-----------------------|
| | $\langle 100 \rangle$ | $\langle 110 \rangle$ | $\langle 111 \rangle$ |
| $[001]$ | 2 | 2 | 1 |
| $[110]$ | 2 | 3 | 2 |
| $[111]$ | 1 | 2 | 2 |

note that the apparent ground-state splitting resulting from the removal of the orientational degeneracy is not accompanied by depopulation effects.

In light of the above discussion, we now present the results of our study on the NTD acceptor centers for $F\parallel[001]$ and $F\parallel[111]$, the polarized light being characterized by $E\parallel F$ or $E\perp F$.

B. $F\parallel[111]$

In Figs. 7 and 8 we display lines 1 and 2 of the NTD and boron acceptors, respectively, for $F\parallel[111]$ and E either parallel or perpendicular to F . The zero-stress positions of lines 1 and 2 are indicated by the vertical arrows and the stress-induced components are labeled according to the nomenclature in Fig. 6. Lines 1 and 2 correspond to transitions from the Γ_8 ground state to the first two Γ_8 excited states of the $p_{3/2}$ series. At low stress (~ 0.12 kbar), the components 1.1 and 1.2 of line 1 and 2.1 and 2.2 of line 2 are clearly observed for both the NTD and boron acceptors, as can be seen in (a) and (b) of Figs. 7 and 8. As the magnitude of the applied stress is increased, the intensity of these components decrease, until

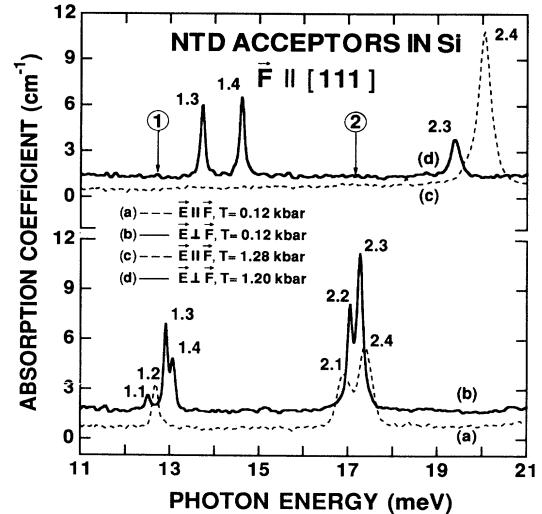


FIG. 7. Effect of uniaxial stress on lines 1 and 2 of NTD acceptors for $F\parallel[111]$ and (a) $E\parallel F$, $T=0.12$ kbar, (b) $E\perp F$, $T=0.12$ kbar, (c) $E\parallel F$, $T=1.28$ kbar, and (d) $E\perp F$, $T=1.20$ kbar. Measurements were performed using liquid helium as coolant.

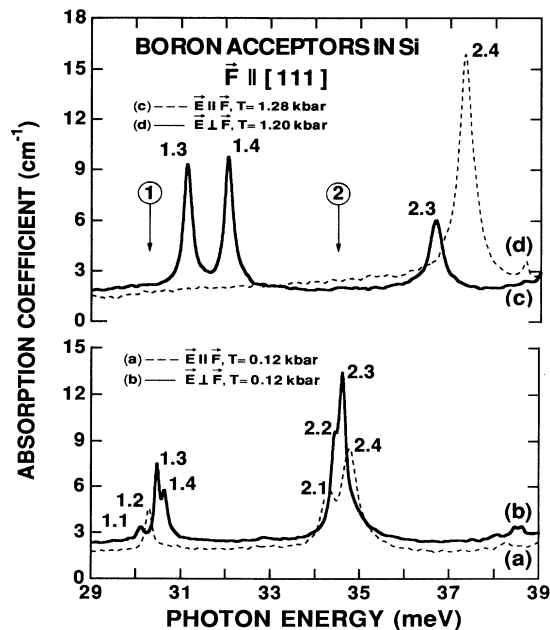


FIG. 8. Effect of uniaxial stress on lines 1 and 2 of boron acceptors for $F||[111]$ and (a) $E||F$, $T=0.12$ kbar, (b) $E\perp F$, $T=0.12$ kbar, (c) $E||F$, $T=1.28$ kbar, and (d) $E\perp F$, $T=1.20$ kbar. Measurements were performed using liquid helium as coolant.

they finally disappear, as illustrated in (c) and (d) of Figs. 7 and 8, where only 1.3, 1.4, 2.3, and 2.4 are present. The decrease in intensity and the final disappearance of 1.1, 1.2, 2.1, and 2.2 at higher stresses are consequences of the depopulation effect and indicate the splitting of the Γ_8 ground state into two Kramers doublets.

Figure 9 shows the stress dependence of the positions of the stress-induced components of lines 1 and 2 of the NTD acceptors. The polarization selection rules depicted in Fig. 6 apply to both the boron and the NTD spectra and fully justify the level ordering under compression as shown therein. The energy spacing between 2.3 and 2.1 as well as that between 2.4 and 2.2 yields the ground-state splitting. Similarly, the spacing between 1.4 and 1.2 as well as that between 1.3 and 1.1 should also correspond to the ground-state splitting.

A close inspection of (c) and (d) in Figs. 7 and 8 reveal unusual changes in the relative intensities of the stress-induced multiplets of lines 1 and 2. The component 2.3 has suffered a dramatic decrease in intensity at the higher stresses, while the intensity of 1.4 has correspondingly increased. As illustrated in Fig. 6, 1.4 and 2.3 correspond to transitions from the Γ_4 sublevel of the ground state to the $\Gamma_5 + \Gamma_6$ sublevels of the excited states of lines 1 and 2, respectively. At sufficiently high stresses these $\Gamma_5 + \Gamma_6$ sublevels will mix, resulting in the large change of intensities observed.³¹ These depopulation and level-crossing effects have been clearly observed and interpreted for the group-III acceptors and the present results illustrate the complete parallel between the NTD and the boron acceptors in this context.

It is interesting to notice the related nonlinearity in the

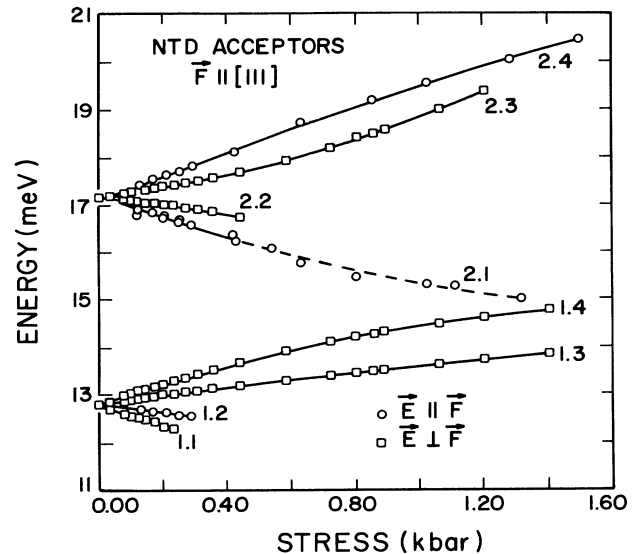


FIG. 9. Stress dependence of the energies of the components of lines 1 and 2 of the NTD acceptors in silicon for $F||[111]$.

stress dependence of the positions of 1.2, 1.4, 2.1, and 2.3. In contrast, these effects are significantly smaller for 1.3 and 2.4 because, although their final Γ_4 states can mix, they move apart with increasing stress as can be seen from Fig. 6. By maintaining the sample at a temperature higher than that of liquid helium, it is possible to have a population in the $\Gamma_5 + \Gamma_6$ ground-state sublevel significant enough to observe transitions originating from it even at higher stresses. In the measurements displayed in Fig. 9, 2.1 was observed up to stresses as high as ~ 1 kbar as indicated by the dashed lines; an inadvertent loss of liquid helium traced to a minor helium leak in the cryostat resulted in warming up the sample to ~ 40 K and in turn enabled the observation of 2.1 at higher stresses.

The stress effects of the NTD centers described above closely follow those observed for boron. This similarity is brought out in Fig. 10 where we show the stress dependence of the lines 1 and 2 of boron, including 2.1 at higher stress as indicated by the dashed lines. We emphasize here the convenient observation of the NTD and the boron excitation lines, with and without stress, in the same experiment, under identical experimental conditions, made possible by the large spectral coverage feasible with the Fourier-transform spectrometer.

C. $F||[001]$

In order to interpret the piezospectroscopic results for the NTD acceptors with $F||[001]$, it is useful to recall³¹ the salient features of the corresponding results for boron acceptors. Figure 6(b) shows the splittings of the Γ_8 levels for $F||[001]$ and the allowed transitions for group-III acceptors in silicon, with the level ordering of the stress-induced sublevels deduced from the polarization and thermal depopulation effects. For example 2.2 and 2.3 of boron coincide for both $E||F$ and $E\perp F$ implying that the Γ_8 ground state and the Γ_8 excited state experience equal

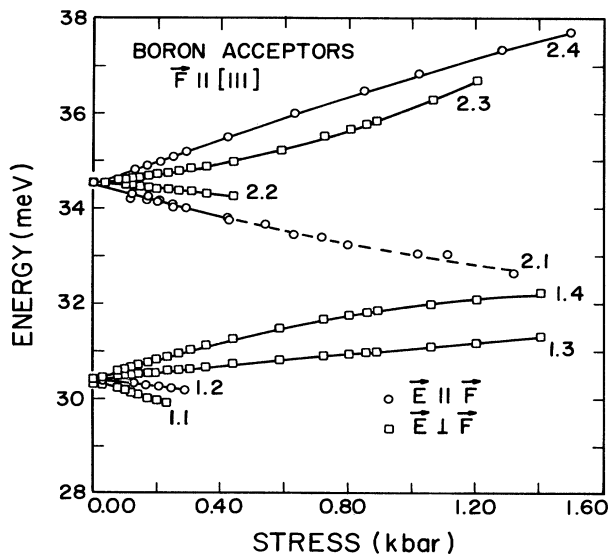


FIG. 10. Stress dependence of the energies of the components of lines 1 and 2 of boron acceptors in silicon for $F||[111]$.

splittings. Therefore, the deformation-potential constant b_2 is equal in magnitude to b_0 but of opposite sign, since the ordering of the excited state sublevels is opposite to that of the ground state sublevels. The components 2.1 and 2.4 are not observed experimentally; their absence has been explained from the theoretical calculations on the intensity of the electric-dipole transitions.³² As a consequence of the very small or experimentally undetectable splitting of the Γ_8 excited state, 1.3 and 1.4 are coincident, so are 1.1 and 1.2. The components 1.1 and 1.2 originate from the upper Kramers doublet of the ground state and therefore show depopulation effects. In Fig. 11 we illustrate these features of lines 1 and 2 of boron acceptors observed in the present measurements on $Si(B, P_{NTD})$ for (a) $E||F$ and (b) $E\perp F$, where the zero-stress positions are indicated by the vertical arrows.

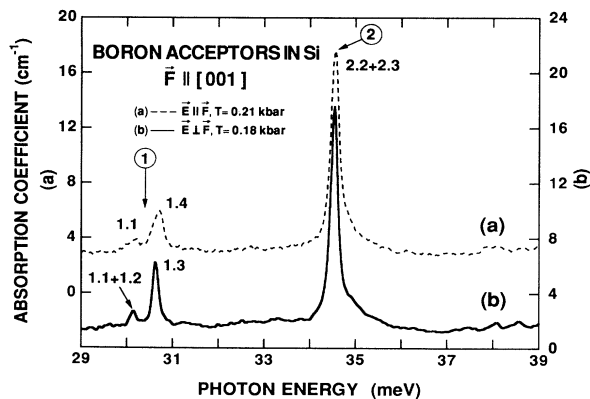


FIG. 11. Effect of uniaxial stress on lines 1 and 2 of boron acceptors in $Si(B, P_{NTD})$ for $F||[001]$ and (a) $E||F$, $T=0.21$ kbar and (b) $E\perp F$, $T=0.18$ kbar. Measurements were performed using liquid helium as coolant.

In Fig. 12 we display lines 1 and 2 of the NTD acceptor for $F||[001]$ and $E\perp F$, where their zero-stress positions are indicated by the vertical arrows. We notice that even for high-stress values 2.3 suffers a relatively small shift from the zero-stress position of line 2, thus closely resembling the corresponding behavior of line 2 of boron. For low to moderate stresses an additional component, labeled 2.2 is observed, which, on the basis of depopulation and polarization features, we attribute to the transition from the upper Γ_6 sublevel of the ground state to the Γ_7 sublevel of the excited state. This additional component is not observed in either $Si(B)$ or $Si(Al)$, but appears in the spectrum of $Si(In)$ (Refs. 27 and 31) for $F||[001]$. However, in contrast to the 2.2 of the NTD acceptors, it occurs on the high energy side of 2.3 in the In spectrum. As in the case of boron acceptors, the components 2.1 and 2.4 are not observed for the NTD centers. The observation of 2.2 and 2.3 and their relative energies indicate that for the NTD acceptor the ground state has suffered a somewhat larger splitting than that of the excited state, whereas for boron, both the ground and the excited state experience equal splittings. Another difference between boron and NTD acceptors, is the occurrence of clearly resolved lines 1.3 and 1.4 in the latter with 1.3 observed for $E\perp F$ and 1.4 for $E||F$. We note here that 1.3 and 1.4 are coincident in $Si(In)$ for both polarizations, whereas in $Si(Al)$ they are resolved; however, 1.3 and 1.4 in Al occur in $E||F$ and $E\perp F$, respectively, in contrast to the case of NTD. From the intensity and polarization features observed for the line 1 components of the NTD acceptors, it is deduced that their stress-induced Kramers doublets follow exactly the level scheme of line 1 as depicted in Fig. 6(b), whereas for $Si(Al)$ the excited states occur in the reverse order, i.e., similar to that for line 2 in the diagram. Due to depopulation effects, 1.1+1.2 and 2.2 are observed in the NTD spectrum only for a narrow range of low-stress values.

Figures 13 and 14 show the positions of the stress-induced components of lines 1 and 2 as function of stress for the NTD and boron acceptors, respectively. Once again, the close similarity in the stress-induced behavior

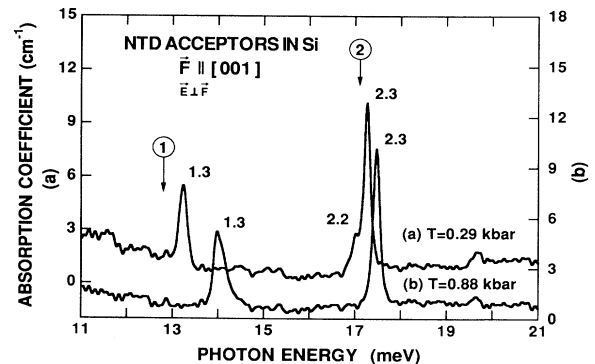


FIG. 12. Effect of uniaxial stress on lines 1 and 2 of the NTD acceptors in silicon for $F||[001]$, $E\perp F$ and (a) $T=0.29$ kbar and (b) $T=0.88$ kbar. Measurements were performed using liquid helium as coolant.

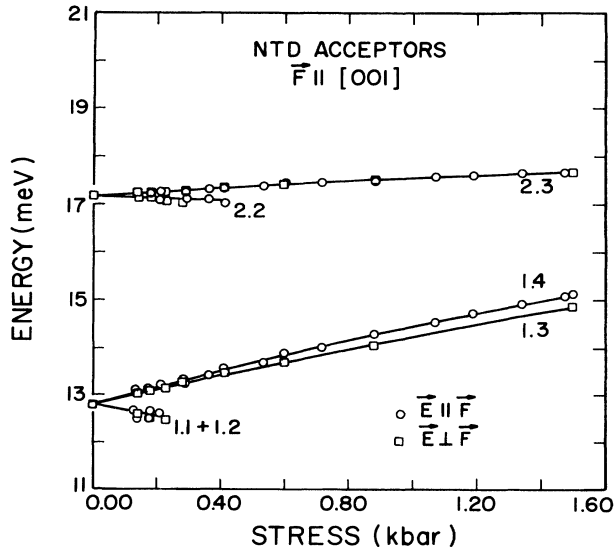


FIG. 13. Stress dependence of the energies of the components of lines 1 and 2 of the NTD acceptor centers in silicon for $F||[001]$.

of lines 1 and 2 for boron and NTD acceptors is evident.

The close similarity in the piezospectroscopic behavior of the NTD and boron acceptors strongly indicates that the NTD centers have the same site symmetry as that of boron, i.e., T_d . The NTD centers do not exhibit any evidence of orientational degeneracy expected from defects of lower symmetry.

D. Deformation-potential constants

We now deduce the deformation-potential constants which quantitatively characterize the splittings and shifts of the energy levels involved in the optical transitions of the acceptor whose piezospectroscopy is under study.

For the Γ_8 ground state, the stress-induced separation between its two sublevels is given by $(d_0/\sqrt{3})s_{44}T$ and $2b_0(s_{11}-s_{12})T$, for $F||[111]$ and $F||[001]$, respectively. For the Γ_8 excited states, there is considerable interaction between adjacent stress-induced sublevels bearing the same symmetry. Such mixing or interaction is taken into account in the theoretical calculations to derive the energy separation between the stress-induced components as function of the applied stress. A complete analysis including the interaction or mixing of states via the strain potential is given in Chandrasekhar *et al.*³¹

In Fig. 6(a), we note that for $F||[111]$ the stress dependence of the energy spacing between 2.3 and 2.1, 2.4 and 2.2, 1.4 and 1.2, and 1.3 and 1.1, all yield the ground-state splitting. In Fig. 15 we plot Δ_{111} , the ground-state splitting, as function of the applied stress and from the slopes of the linear least-squares fits to these curves, deduce d_0 for both NTD and B. The slopes are 3.54 ± 0.02 meV/kbar and 3.17 ± 0.03 meV/kbar for NTD and B, respectively. In Table V we list the d_0 values resulting from our present investigation together with those reported in the literature.^{31,33,34}

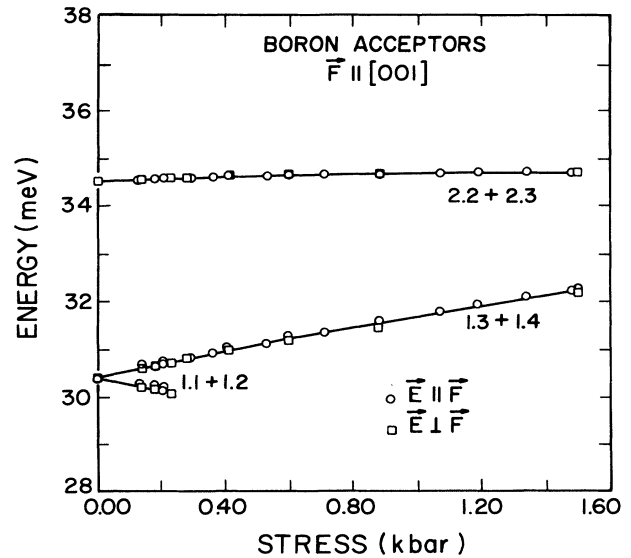


FIG. 14. Stress dependence of the energies of the components of lines 1 and 2 of boron in silicon for $F||[001]$.

A similar procedure was used to determine b_0 from the measurements for $F||[001]$, with the stress dependence of the energy spacing between 1.4 and 1.2, and 1.3 and 1.1, yielding the ground-state splitting [Δ_{100} as shown in Fig. 6(b)]. Due to depopulation effects 1.1 and 1.2 could be

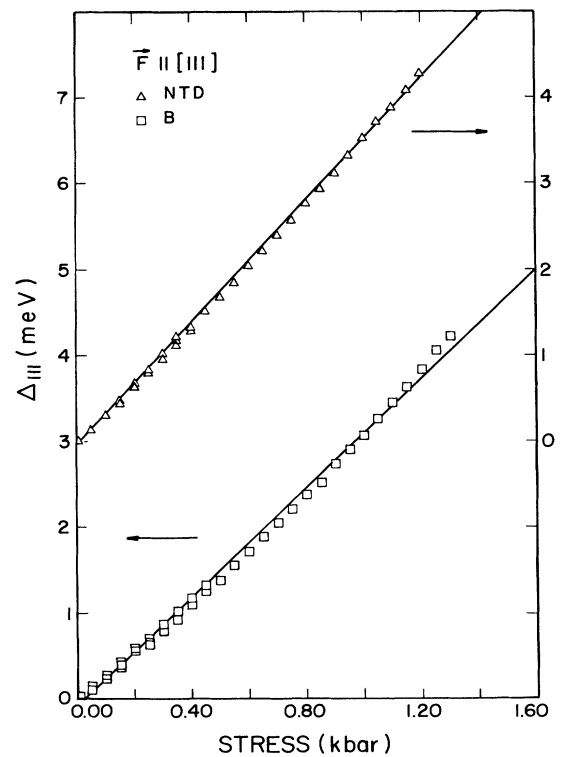


FIG. 15. The ground-state splitting (Δ_{111}) deduced from the energy spacing (2.3-2.1), (2.4-2.2), (1.4-1.2), and (1.3-1.1) as a function of stress for $F||[111]$. The straight line passing through the data points represents a least-squares fit.

TABLE V. Deformation-potential constants of the ground state of B and of NTD acceptors in Si.

| Ref. | d_0 (B) (eV) | b_0 (B) (eV) | $(d_0/b_0):B$ | d_0 (NTD) (eV) | b_0 (NTD) (eV) | $(d_0/b_0):NTD$ |
|------|-------------------|-------------------|---------------|---------------------|---------------------|-----------------|
| a | -4.41 ± 0.04 | -1.41 ± 0.06 | 3.13 | -4.92 ± 0.05 | -1.55 ± 0.07 | 3.17 |
| b | -4.50 ± 0.15 | -1.61 ± 0.07 | 2.80 | | | |
| c | -4.02 ± 0.09 | -1.38 ± 0.04 | 2.91 | | | |
| d | -3.32 | -1.23 | 2.70 | | | |

^aPresent work.

^bChandrasekhar *et al.* (Ref. 31).

^cLewis, Fisher, and McLean (Ref. 33).

^dBuczko (Ref. 34).

observed for stresses only up to ~ 0.20 kbar. In this stress range, 1.3 and 1.4 are almost coincident, as are 1.1 and 1.2, due to the very small splitting of the excited state. Therefore, b_0 was extracted from the energy spacing between $1.3+1.4$ and $1.1+1.2$ and as illustrated in Fig. 16, the slopes are 3.03 ± 0.13 meV/kbar and 2.74 ± 0.12 meV/kbar for NTD and B, respectively; the b_0 values are listed in Table V.

Table V compares our values of b_0 and d_0 with those obtained by Chandrasekhar *et al.*³¹ and Lewis, Fisher, and McLean³³ using an identical experimental approach. Also listed are the theoretical values of b_0 and d_0 as calculated by Buczko³⁴ using the effective-mass theory. Although the experimental values are in general agreement amongst one another, the origin of the differences is not

clear. The data for $F||[111]$ are more extensive, especially for line 2, allowing a more precise determination for the value of d_0 , which appears to show a good agreement with previously published results. On the other hand, our data for $F||[001]$ are limited to stresses up to ~ 0.20 kbar, thus contributing to the differences observed for the values of b_0 . We also have to keep in mind that the very small splitting of the final state of line 1 may have contributed to the uncertainty in determining Δ_{100} . On the other hand, when Δ_{100} is determined from the splitting of the $2p'$ line of the $p_{1/2}$ series, as deduced by Chandrasekhar *et al.*,³¹ the procedure is free from this limitation since the final state of $2p'$ is only a Kramers doublet.

The theoretical calculations of Buczko for the effective-mass "acceptor" gives $b_0 = -1.23$ eV and $d_0 = -3.32$ eV. These are to be compared with values for Al, which is isocoric with Si, and hence the most effective-mass-like. We note that the d_0 for B is significantly higher than the experimentally observed³¹ value for Al, whereas Buczko's calculated value for d_0 does agree with that for the latter within 15%. It appears that shallower the acceptor, the larger the value of d_0 . We also note that In, the deepest acceptor, has markedly lower values for b_0 and d_0 .

Chandrasekhar *et al.*³¹ experimentally observed that the splitting of the ground state for different directions of stress, in particular, for $F||[001]$, $[110]$, and $[111]$ is the same for a given stress. The anisotropy of the ground state³¹ is given by $\Delta^2(\alpha_x, \alpha_y, \alpha_z) = \Delta_{100}^2 + 3(\Delta_{111}^2 - \Delta_{100}^2)K(\alpha_x, \alpha_y, \alpha_z)$, with $K(\alpha_x, \alpha_y, \alpha_z) = \alpha_x^2 \alpha_y^2 + \alpha_y^2 \alpha_z^2 + \alpha_z^2 \alpha_x^2$, α_x , α_y , and α_z being the direction cosines of F . If $|\Delta_{100}| = |\Delta_{111}|$, it is clear that identical ground-state splitting will occur for the same applied stress, irrespective of the direction of the force, i.e., a behavior characterized by the label "stress isotropy." For Si, stress isotropy results when $d_0/b_0 = 2.71$; this ratio is also compared for different measurements and Buczko's theory in Table V. Again, while qualitatively indicating stress isotropy, the different sets are not entirely mutually consistent. We also note that stress isotropy of the valence-band maximum was first noticed by Thomas³⁵ in his study of the piezospectroscopy of the free exciton of CdTe.

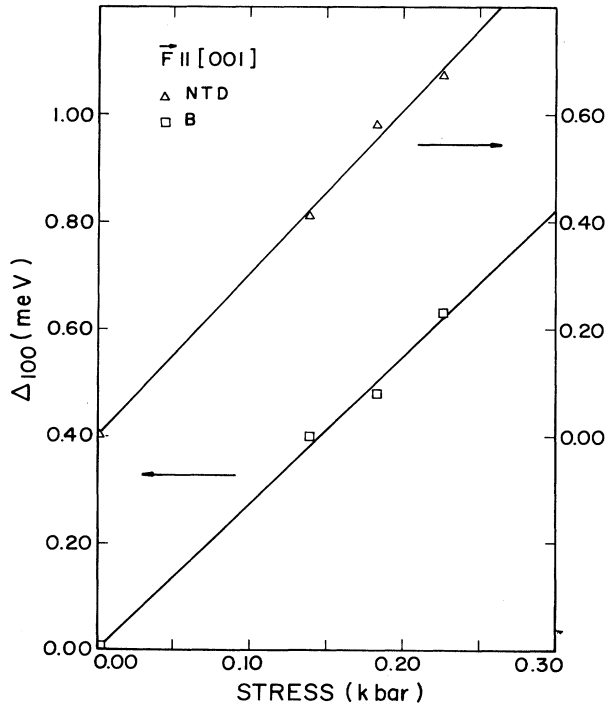


FIG. 16. The ground-state splitting (Δ_{100}) deduced from the energy spacing $(1.3+1.4)-(1.1+1.2)$ as a function of stress for $F||[001]$. The straight line passing through the data points represents a least-squares fit.

VI. CONCLUDING REMARKS

The present studies have shown that ultrashallow NTD acceptor centers occur in Si in association with B or Al

acceptors present in the starting material. The electrical measurements of Young *et al.*²³ on Si doped with Al, In, Ga, and subjected to neutron irradiation, also revealed two shallow levels in Si(Al,P_{NTD}) with ionization energies of 30 and 41 meV. From our spectroscopic results we identify the former with B_{NTD} centers, where the B is presumably the common residual impurity, and the latter with Al_{NTD}. The occurrence of NTD centers in association with In and Ga acceptors has yet to be established. The appearance of the NTD lines in the early stages of annealing and their final disappearance at temperatures higher than $\sim 725^\circ\text{C}$ indicate diffusion and formation of defect complexes in association with the group-III acceptors already present in the material; these defects could probably be generated by the neutron transmutation itself and/or by the fast-neutron component of the neutron flux. We note here that in the present study $\sim 10\%$ of the neutron flux consisted of fast neutrons which could have easily produced vacancies and interstitials in sufficient concentration to account for the NTD centers. It is also likely that such shallow NTD centers can be created by subjecting the sample to the proper flux of high energy neutrons or electrons and subsequent annealing; further systematic investigations are necessary to determine clearly the factors responsible for the formation of the NTD centers.

The spectroscopic measurements yielded ionization energies of $E_I(\text{B}_{\text{NTD}})=28.24$ meV and $E_I(\text{Al}_{\text{NTD}})=43.25$ meV for B_{NTD} and Al_{NTD} centers, respectively. The near coincidence of the ratios between the ionization energies of the NTD center with that of the corresponding acceptor, viz., $E_I(\text{B}_{\text{NTD}})/E_I(\text{B})=0.618$ and $E_I(\text{Al}_{\text{NTD}})/E_I(\text{Al})=0.616$, again strongly indicates that the NTD center is associated with the specific "parent" group-III acceptor.

The piezospectroscopic measurements have revealed that the NTD centers possess T_d site symmetry; this is an unexpected result since, in general, it is found that complex defects in Si have a site symmetry lower than that of the group-III substitutional acceptors. The tetrahedral symmetry associated with the NTD centers raises the possibility of four defects grouping together to form the NTD center, a highly surprising circumstance, e.g., interstitials around the substitutional B. Given the sharpness and the consistent reproducibility of the NTD excitation lines from sample to sample, it appears unlikely that *large* clusters of interstitials could ensure the tetrahedral sym-

metry and the small ionization energy of the NTD centers. One could speculate that a strain field around the substitutional acceptor impurity results from the neutron transmutation of ³⁰Si and/or the fast-neutron damage; however this hypothesis too appears highly improbable in view of the sharpness and the reproducibility of the excitation spectra. It is clear that the details of the microscopic nature of the NTD center have yet to be conclusively determined.

At this point it is important to recall the theoretical results involving shallow acceptors in both Si and Ge. The isocoric acceptors, Al in Si and Ga in Ge, are predicted to be the most effective-mass-like of the group-III substitutional impurities and therefore, the shallowest. The fact that B is shallower than Al has been attributed by Lipari and Baldereschi²⁴ to an exclusion of the hole from the vicinity of the acceptor center, i.e., the ground-state binding energy of Si(B) suffers a *negative* chemical shift because of a repulsive component of the potential. It appears that, in the NTD center, this effect is even further accentuated thus leading to the markedly low binding energies observed.

It is useful to compare the NTD centers with *X* centers, which occur in both Czochralski and floating-zone-grown silicon doped with group-III acceptors.^{27,29} The ionization energies of the *X* centers are $\sim 70\text{--}80\%$ of those of the corresponding group-III impurities and the *X* centers do not anneal out at high temperatures. It has been shown that Al-*X* centers have trigonal site symmetry,²⁸ in contrast to the B_{NTD} centers which have tetrahedral site symmetry as the present studies have shown.

Finally, it is useful to appreciate that the low ionization energy of the NTD centers in silicon, identified in the present work, together with their reproducibility from sample to sample in a controlled fashion, could be exploited in designing a far-infrared photoconductive detector.

ACKNOWLEDGMENTS

We thank Dr. John Farmer for the slow-neutron irradiation of the silicon samples, performed at the Research Reactor Facility, University of Missouri, Columbia, Missouri. The present investigation was supported by a grant from the National Science Foundation (Grant No. DMR-89-21717).

*Present address: Sun Microsystems, Inc., 621 Columbia Street Extension, Cohoes, NY 12047.

¹A. K. Ramdas and S. Rodriguez, Rep. Prog. Phys. **44**, 1297 (1981).

²W. Kaiser, P. H. Keck, and C. F. Lange, Phys. Rev. **101**, 1264 (1956); W. Kaiser, H. L. Frisch and H. Reiss, *ibid.* **112**, 1546 (1958).

³M. Stavola, K. M. Lee, J. C. Nabity, P. E. Freeland, and L. C. Kimerling, Phys. Rev. Lett. **54**, 2639 (1985); M. Stavola, in

Proceedings of the Second International Conference on Shallow Impurity Centers, edited by A. Baldereschi and R. Resta (North-Holland, Amsterdam, 1987), p. 187.

⁴J. J. Gilman, *The Art and Science of Growing Crystals* (Wiley, New York, 1963); R. A. Laudise, *The Growth of Single Crystals* (Prentice-Hall, Englewood Cliffs, NJ, 1970); A. J. R. de Koch, in *Handbook on Semiconductors*, edited by S. P. Keller (North-Holland, Amsterdam, 1980), Vol. 3.

⁵H. Reiss and C. S. Fuller, in *Semiconductors*, edited by N. B.

- Hannay (Reinhold, New York, 1960), pp. 222–268.
- ⁶For a review, see, for example, K. A. Pickar, in *Ion-implantation in Silicon—Physics, Processing and Microelectronic Devices*, edited by R. Wolfe, Applied Solid State Science Vol. 5 (Academic, New York, 1975), p. 151.
- ⁷C. Jagannath, Z. W. Grabowski, and A. K. Ramdas, *Solid State Commun.* **29**, 355 (1979); C. Jagannath, Z. W. Grabowski, and A. K. Ramdas, *Phys. Rev. B* **23**, 2082 (1981).
- ⁸A preliminary account was presented in C. R. LaBrec, M. K. Udo, and A. K. Ramdas, *Appl. Phys. Lett.* **52**, 1505 (1988) and M. K. Udo, C. R. LaBrec, and A. K. Ramdas, *Bull. Am. Phys. Soc.* **35**, 279 (1990).
- ⁹Beckman Instruments, Inc., 2500 Harbor Blvd., Fullerton, CA 92634.
- ¹⁰Infrared Laboratories, Inc. 1808 E 17th St., Tucson, AZ 86719.
- ¹¹Zenith Data Systems, St. Joseph, MI 49085.
- ¹²P. Fisher, W. H. Haak, E. J. Johnson, and A. K. Ramdas, in *Proceedings of the Eighth Symposium on the Art of Glass Blowing* (The American Scientific Glass Blowers-Society, Wilmington, Delaware, 1963), p. 136.
- ¹³V. J. Tekippe, H. R. Chandrasekhar, P. Fisher, and A. K. Ramdas, *Phys. Rev. B* **6**, 2348 (1972).
- ¹⁴L. H. Johnston, *Appl. Opt.* **16**, 1082 (1977); C. J. Jagannath, Ph.D. thesis, Purdue University, 1980.
- ¹⁵Polyethylene wire-grid polarizer model 186-0082, manufactured by Perkin-Elmer Corp., Norwalk, CT.
- ¹⁶Irradiation performed at the Research Reactor Facility, University of Missouri, Columbia, Missouri, through the courtesy of Dr. John Farmer.
- ¹⁷K. Lark-Horovitz, in *Semi-Conducting Materials*, edited by H. K. Henish (Butterworths, London, 1951), p. 47.
- ¹⁸M. Tanenbaum and A. D. Mills, *J. Electrochem. Soc.* **108**, 173 (1961).
- ¹⁹S. L. Gun, J. M. Meese, and D. M. Alger, in *Neutron Transmutation Doping in Semiconductors*, edited by J. M. Meese (Plenum, New York, 1979), p. 197.
- ²⁰J. M. Meese, D. L. Cowan, and M. Chandrasekhar, *IEEE Trans. Nucl. Sci. NS* **-26**, 4858 (1979).
- ²¹H. J. Stein, in *Radiation Effects in Semiconductors*, edited by J. W. Corbett and G. D. Watkins (Gordon and Breach Science, New York, 1971), p. 125; J. M. Meese, in *Neutron Transmutation Doping in Semiconductors*, edited by J. M. Meese (Plenum, New York, 1979), p. 1.
- ²²B. C. Larson, R. T. Young, and J. Narayan, in Ref. 19, p. 281.
- ²³R. T. Young, J. W. Cleland, R. F. Wood, and M. M. Abraham, *J. Appl. Phys.* **49**, 4752 (1979); J. W. Cleland, P. H. Fleming, R. D. Westbrook, R. F. Wood, and R. T. Young, in Ref. 19, p. 261.
- ²⁴A. Baldereschi and N. O. Lipari, in *Physics of Semiconductors*, edited by F. G. Fumi (Tipografia Marves, Rome, 1976), p. 595; N. O. Lipari and A. Baldereschi, *Solid State Commun.* **25**, 665 (1978).
- ²⁵M. C. Ohmer and J. E. Lang, *Appl. Phys. Lett.* **34**, 750 (1979).
- ²⁶M. H. Young, O. J. Marsh, and R. Baron, Ref. 19, p. 335.
- ²⁷A. Onton, P. Fisher, and A. K. Ramdas, *Phys. Rev.* **163**, 686 (1967).
- ²⁸H. R. Chandrasekhar and A. K. Ramdas, *Phys. Rev. B* **33**, 1067 (1986).
- ²⁹C. E. Jones, D. Schafer, W. Scott, and R. J. Hager, *J. Appl. Phys.* **52**, 5148 (1981), and references cited therein.
- ³⁰G. F. Koster, J. O. Dimmock, R. G. Wheeler, and H. Statz, *Properties of the Thirty-two Point Groups*, (MIT, Cambridge, MA, 1963).
- ³¹H. R. Chandrasekhar, P. Fisher, A. K. Ramdas, and S. Rodriguez, *Phys. Rev. B* **8**, 3836 (1973).
- ³²S. Rodriguez, P. Fisher, and F. Barra, *Phys. Rev. B* **5**, 2219 (1972).
- ³³R. A. Lewis, P. Fisher, and N. A. McLean, in *Shallow Impurities in Semiconductors 1988*, edited by B. Monemar (Institute of Physics, Bristol, 1989), p. 95.
- ³⁴R. Buczko, *Il Nuovo Cimento* **9**, 669 (1987).
- ³⁵D. G. Thomas, *J. Appl. Phys.* **32**, 2298 (1961).